STRUCTURE AND PROPERTIES OF PM Fe-B-Si COMPACTS AFTER THROUGH VACUUM CARBURIZING

K. Widanka

Abstract

The paper presents structural and strength characteristics of sintered steels obtained by through vacuum carburizing of iron compacts with additions of boron and silicon.

Vacuum carburizing with immediate sintering of the compacts made of a mixture of iron ASC100.29, ferroboron and silicon powders was carried out at 1050 and 1150°C in a laboratory vacuum furnace.

The effect of silicon on the structure of surface layer and core, as well as selected mechanical properties of the obtained sintered alloys was analysed. It was evidenced that a silicon addition up to 1 % ensured the best mechanical properties of the examined steel specimens.

Keywords: vacuum carburizing; iron-boron-silicon compacts; microstructure; mechanical properties; sintered steels

INTRODUCTION

Both boron and silicon as alloying elements are rarely present in PM iron alloys. Silicon has a relatively high solubility in Fe_α, decreasing with temperature from 18.5 % for the temperature range within 1020 to 1200°C down to 15% at ambient temperature. Maximum solubility of silicon in Fe_γ is ca 2 %[1]. At higher concentration than 2.15 %, γ-iron no longer exists in Fe-Si alloys.

Boron dissolves in ferrite and also in austenite in very low amounts. Maximum solubility of boron in Fe_γ is ca 0.02 % at the temperature range within 1100 to 1200ºC [2]. Both silicon and boron decrease the solubility of carbon in austenite.

In sintered steels, silicon as an alloying element is most often present in alloyed stainless steels with Cr and in acid-resisting steels with Cr, Ni and Mo in percentages up to 1% [3]. Another significant group of the materials manufactured by powder metallurgy, where silicon is used as the main alloying additive, are iron-based soft magnetic materials. In these alloys, silicon is added to iron powder in a quantity within 1% to 4% (Fe-Si alloys) or 1% to 3% (Fe-Si-P alloys) [3].

Boron is introduced to wrought structural steels mainly to improve their hardenability. In sintered steels, boron mostly plays another role: it intensifies the sintering process by creating a liquid phase at the sintering temperature as a result of the eutectic reaction (ferrite with iron boride Fe_2B). Thereby, it increases density of the sintered compacts and, as a consequence, improves their mechanical properties [4-7].

The vacuum carburizing may be used for sintered materials due to better control of carburizing depth in comparison with conventional gas carburizing. This allows obtaining the required thickness of carburized layer in more predictable way. The method ensures a faster carburizing course, mainly thanks to higher temperature and lower hydrocarbon gas pressure during the process [8-12].

Krzystof Widanka, Wroclaw University of Technology, Institute of Materials Science and Applied Mechanics, Materials Science Division, Wroclaw, Poland

The carburizing depth depends on the carbon diffusion rate into the material, which depends on process parameters and also on the carburized material. The carbon diffusion rate in iron and iron alloys is decided by its diffusion coefficient, which for carburizing processes carried out at high temperatures (above 1000°C) is more than two times larger than for traditional gas carburizing [13]. An addition of silicon in these alloys increases the carbon diffusion coefficient. Experimental data related to the effect of boron on carbon diffusion parameters in steels are limited due to very low solubility of boron both in ferrite and in austenite. All the available data [14-16] confirm that boron addition increases carbon activity in the Fe-C-B alloys. This allows one to assume that an additive of boron increases the carbon diffusion coefficient like silicon.

In this paper, the effect of both mentioned additives on structure and selected mechanical properties of through-carburized iron compacts is presented. Compacts with constant content of boron, equal to about 0.005%, and silicon content ranging from 0.5 to 2.0% were pressed to a lowest density of 7.2 g/cm^3 in order to minimize the interconnected porosity.

Carburizing of the compacts carried out in a vacuum furnace was accompanied by the sintering process. This way, sintered steels were obtained, with variable carbon content on their cross-sections. The sinters obtained as such were subjected to structural examination of the surface layer and core, hardness measurements and a tensile test to determine their basic mechanical properties.

MATERIAL AND EXPERIMENT

Standard flat specimens for mechanical testing with shape and dimensions: 5.85 x 6.05 mm (in gage section) according to ISO 2740 were prepared of a mixture of iron powder ASC100.29 (by Höganäs AB), ferroboron FeB16 powder and silicon powder Si AX0.5 (by H.C. Starck) with an average particle size equal to 3.5 μm. Double-sided compacting under pressure within 750 to 800 MPa was applied to obtain compacts with the lowest density of 7.2 g/cm^3. Their chemical composition and green density, which was measured by means of the Archimedes method, are given in Table 1.

The vacuum carburizing process was carried out in a laboratory vacuum furnace (made by Seco/Warwick). Parameters of the process were based on the results of our own research, to obtain surface carbon content within the range 0.7 % to 0.8 %. The selected parameters are given in Table 2.

The carburizing atmosphere consisted of propane diluted with nitrogen. Working pressure in the furnace chamber was 2 kPa. Stable working pressure in the chamber during carburizing was maintained by cyclic dosing the gas with a constant flow rate of 110 dm^3/h. Cooling rate in nitrogen was 7°C/s. A diagram of the vacuum carburizing process is shown in Fig.1.

Tab.1. Chemical composition and density of compacts.

Specimen	Chemical composition			„green" density [g/cm^3]
	Wt. % B	wt % Si	Wt. % Fe	
Fe-B-0.5Si	0.005	0.5	remainder	7.27
Fe-B-1.0Si		1.0	remainder	7.23
Fe-B-1.5Si		1.5	remainder	7.22
Fe-B-2.0Si		2.0	remainder	7.20

Tab.2. Parameters of vacuum carburizing.

Carburizing temperature [°C]	Carburizing time [min]	Diffusion temperature [°C]	Diffusion time [min]	Total carburizing time [min]
1050	60	1150	120	180

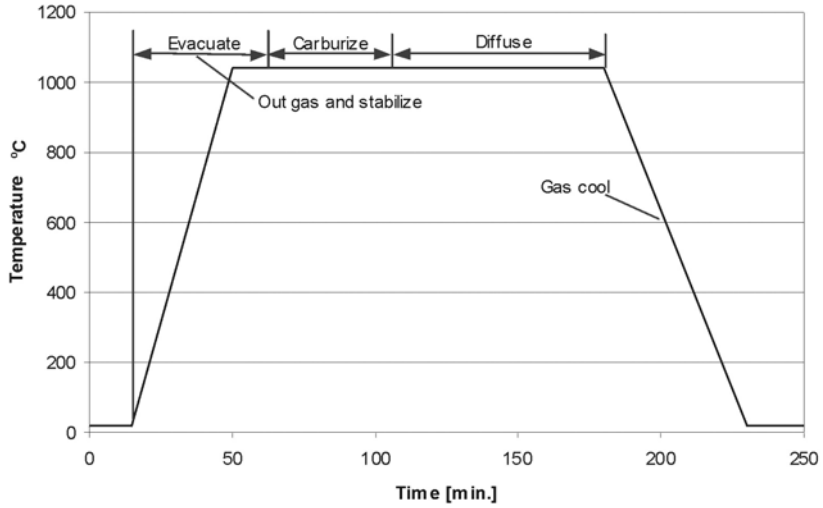

Fig.1. Schematic diagram of vacuum carburizing process.

The specimens for structural examinations were taken from the specimens for mechanical tests after carburizing, by cutting fragments of their measurement parts. Metallographic cross-sections were made on transverse cross-sections of the specimens.

Microscopic examination of the specimens were performed using a light microscope Neophot 32 (by Zeiss), at magnification between 100 to 500 times. Quantitative parameters of the microstructure were evaluated using a computerised image-analysis system "Multiscan" made by the Polish company Computer Scanning Systems. For each specimen a minimum of five (5) images of microstructure were analysed.

Hardness measurements were taken using a hardness tester Zwick by the Vickers method at a load between 9.81 to 49.05 N.

Tensile tests of three specimens at each silicon content were performed on a hydraulic pulsator MTS 810.

RESULTS AND DISCUSSION

In an unetched condition, the porosity degree of the carburized samples was determined by microscopic method using a computerised image analyser. For each sample a minimum of ten (10) images of pores from the whole cross-section were analysed. The obtained results and, evaluated on their grounds, densities of the specimens are presented in Table 3. Figure 2 shows a representative view of pores in the specimen Fe-B-0.5Si (0.5% Si).

Tab.3. Porosity and density of specimens.

Specimen	Porosity [%]	Density [g/cm^3]
Fe-B-0.5Si	6.5	7.36
Fe-B-1.0Si	7.0	7.32
Fe-B-1.5Si	7,2	7.30
Fe-B-2.0Si	7.5	7.28

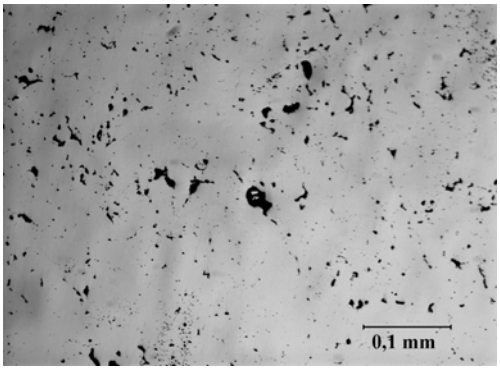

Fig.2. Representative picture of pores in the specimen Fe-B-0.5Si (with 0.5% Si).

Hardness was measured in two zones: in the surface layer and in the core. To determine the hardness profile, measurements were also taken on the cross-section along the centre line from the surface to the core every 0.25 mm.

The obtained hardness measurements permitted determining the thickness of the carburized layers. It was assumed that carburization depth corresponds to mean hardness (HV5) calculated as an arithmetic average of the values for surface layer and core. The so calculated carburization depth values for all the specimens are presented in Table 4. The average thickness of carburized layer of ca 2 mm is comparable for all the examined specimens. A slightly larger value (by ca 0.2 mm) was found for the specimens Fe-B-1.0Si (1.0% Si).

Hardness values for surface layers and cores of the specimens are given in Table 4 and a representative hardness profile for the specimen Fe-B-1.0Si (1.0% Si) is shown in Fig.3. The measured average values for the surface layer are within 189 to 193 HV5 and the values for the core are within 102 to 114 HV5. Larger differences between individual specimens occur in the core than on the surface. The course of hardness profiles is characterised by a wide and round transition from the surface layer to the core, which evidences a smooth drop of carbon content in the carburized layer.

Tab.4. Hardness and thickness of carburized layer of the specimens.

Specimen	Hardness		Thickness of carburized layer [mm]
	of carburized layer HV5	of core HV5	
Fe-B-0.5Si	193 ± 6	102 ± 3	2.1±0.1
Fe-B-1.0Si	189 ± 7	108 ± 2	2.3±0.1
Fe-B-1.5Si	191 ± 6	110 ± 1	2.0±0.1
Fe-B-2.0Si	192 ± 4	114 ± 1	2.0±0.1

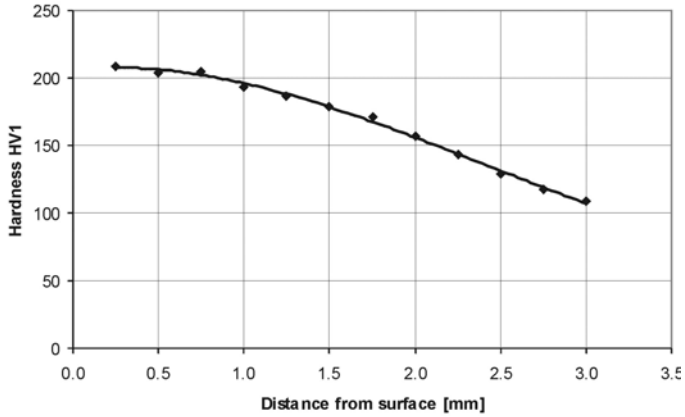

Fig.3. Representative hardness profile for specimen Fe-B-1.0Si.

After etching with 3% nital, the material microstructure of the specimens was revealed. Representative microstructures of carburized layers and cores of the specimens Fe-B-0.5Si and Fe-B-2.0Si are shown sequentially in Figs.4, 5, 6 and 7.

Microstructure of the surface layer of the specimens Fe-B-0.5Si (0.5% Si) consists of pearlite and small amount of cementite ($Fe_3(CB)$) precipitated on prior-austenite grain boundaries during cooling, see Fig.4. In the microstructure of the specimens Fe-B-1.0Si (1.0% Si), pearlite alone was observed.

Microstructure of surface layer of the specimens Fe-B-1.5Si and Fe-B-2.0Si (1.5% Si and 2.0% Si, respectively) consists of pearlite with a small amount of ferrite (Fig.6) that fraction in the structure increases with increasing the silicon content. Microstructure of transition zone in all the specimens consists of pearlite and ferrite, that fraction increases with increasing distance from the surface layer.

The core microstructure of all the specimens consists mainly of ferrite with a small amount of pearlite, that fraction changes depending on the silicon content, from the highest 21% for the specimen Fe-B-1.0Si to the smallest 8% for the specimen Fe-B-2.0Si.

Fractions of pearlite and the, calculated on their grounds, carbon concentrations in the core structure are presented in Table 5. The carbon concentrations were calculated accepting 0.77% C in the eutectoidal point and omitting the silicon effect that shifts it to the left (according to data in literature), towards a lower carbon concentration. With this effect considered, the calculated carbon concentrations would be slightly lower.

Tab.5. Estimated fractions of pearlite and corresponding carbon contents in the cores of the specimens.

Specimen	Pearlite fraction [%]	Carbon content [wt. %]
Fe-B-0.5Si	18	0.14
Fe-B-1.0Si	21	0.16
Fe-B-1.5Si	14	0.11
Fe-B-2.0Si	8	0.06

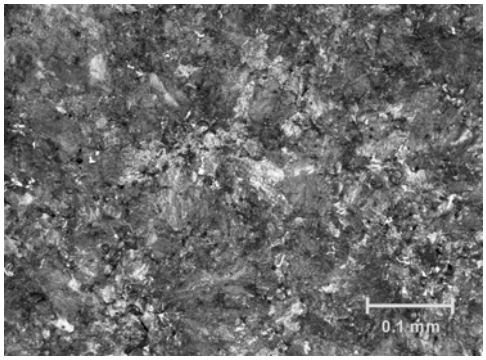

Fig.4. Carburized layer microstructure of the specimen Fe-B-0.5Si (0.5% Si). Magnification 200x.

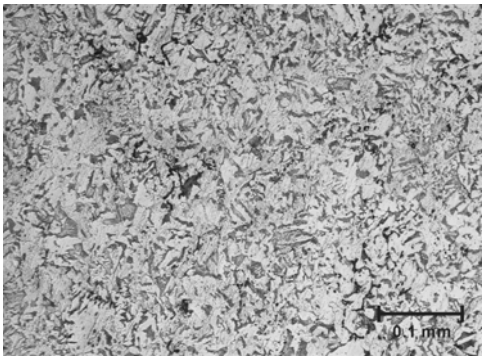

Fig.5. Core microstructure of the specimen Fe-B-0.5Si (0.5% Si). Magnification 200x.

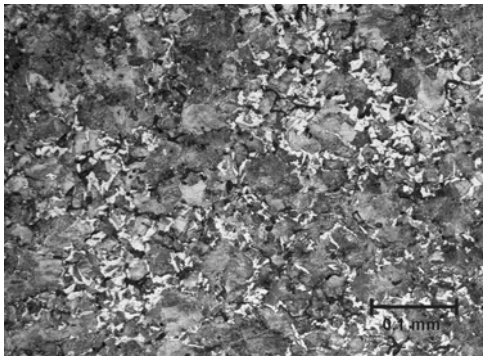

Fig.6. Carburized layer microstructure of the specimen Fe-B-2.0Si (2.0% Si). Magnification 200x.

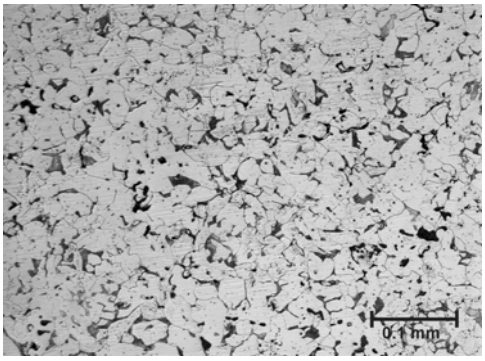

Fig.7. Core microstructure of the specimen Fe-B-2.0Si (2.0% Si). Magnification 200x.

The presence of ferrite in the surface layer structure of the specimens containing 1.5% and 2.0% Si evidences carbon concentration lower than that assumed (0.8% C). This probably results from the lower carbon concentration in the surface layers of these specimens during the boost time, in comparison to the values in the specimens with 0.5%Si and 1.0% Si. This is because silicon increases carbon activity reducing its solubility in austenite and thus decreases its surface concentration in the carburized layer. In the same way it affects the boron. At the carburizing temperature, boron in the specimens is almost completely dissolved in Fe_γ (according to [17], maximum solubility in Fe_γ at 1050°C is ca 0.004%).

In this way, silicon and boron on one side contributes to reducing the carbon stream for diffusion and on the other side it intensifies carbon flow from the carburized layer to the core by increasing its diffusion coefficient. The smaller surface carbon concentration in the carburized layer, the lower is its diffusion rate deep into the material. A quantity of carbon too small for diffusion causes that, in spite of a higher carbon diffusion coefficient in the presence of silicon and boron, the carburizing depth is smaller in the compacts with silicon content over 1% than in those with silicon content up to 1%. This is also proven by the measured pearlite fraction in the core structure of the examined specimens, see Table 5.

The size of pearlite and ferrite grains in the surface layer and core is similar in all the examined specimens. The grains in the layer are larger than those in the core. The pearlite grain size evaluated by comparative method corresponds to the reference standard No. 6 according to ASTM and the ferrite grain size to the standard No. 8.

Basic mechanical properties of the specimens after vacuum carburizing were determined in a static tensile test. The results are presented in Table 6.

Tab.6. Results of tensile test of the examined specimens.

Specimen	UTS* [MPa]	YS* [MPa]	Elongation* [%]
Fe-B-0.5Si	611 ± 7	409 ± 2	4.3 ± 0.2
Fe-B-1.0Si	635 ± 8	414 ± 2	3.2 ± 0.1
Fe-B-1.5Si	602 ± 8	419 ± 3	2.6 ± 0.1
Fe-B-2.0Si	598 ± 9	423 ± 3	1.7 ± 0.2
* - Average value for three tests (three specimens)			

The highest ultimate tensile strength was obtained for the specimens Fe-B-1.0Si and the lowest for the specimens Fe-B-2.0Si. Yield strength increases with increasing silicon content from the lowest value 409 MPa for the specimens Fe-B-0.5Si to the highest 423 MPa for the specimens Fe-B-2.0Si. In turn, elongation decreases with increasing silicon content. The higher tensile strength of the specimens with lower silicon content (≤ 1.0% Si) is a direct consequence of the pearlitic structure (with no ferrite) in the surface layer and larger pearlite fraction in the core structure. Larger pearlite fraction in the core results from deeper diffusion of carbon into the material (larger carburizing depth).

The drop of tensile strength of the specimens with silicon content over 1%, caused by larger and larger fraction of ferrite beside pearlite in the surface layer and smaller pearlite content in the core is partially compensated by the strengthening effect of silicon (solid-solution strengthening of ferrite). Silicon, dissolved mostly in ferrite, increases its strength and, at the same time, reduces its plasticity. This effect is confirmed by the obtained results of the yield stress and elongation (Table 6), as well as hardness measurements of the examined specimens (Table 4).

When comparing the obtained results with the properties of sintered steels produced by the traditional method (of mixtures of iron and graphite powders) based on the ASC100.29 powder of a similar density, it can be seen that they correspond to carbon concentration of 0.5 to 0.7% (constant on the entire cross-section). In addition, these steels include ca 2.0% of copper. According to the database CASIP 5.1 (by Höganäs), tensile strength of these steels is ranging from 534 MPa to 663 MPa, yield stress from 356 MPa to 414 MPa and elongation from 4.8% to 3.6%. So they are close to the properties of the examined sintered steels with carbon content and structure changing on their cross-section. It is only the changing structure that can be profitable for possible application of these steels, e.g. in the manufacture of small-sized gears, especially after strengthening by additional heat treatment.

CONCLUSIONS

Application of the vacuum carburizing method to iron compacts permits combining the carburizing and sintering operations in one process. By proper selection of the process parameters, carbon was introduced to the entire volume of the iron compacts containing additions of boron and silicon.

The advantageous effect of the high temperature of the process on increasing the carbon diffusion coefficient resulted in an accelerated diffusion of carbon deep into the material, and in carburizing the compacts through in a relatively short time. This enabled obtaining specimens of sintered steels with variable carbon content on their cross-section and thus with variable structure.

The highest tensile strength was obtained for the specimens Fe-B-1.0Si (1.0% Si). This results from the purely pearlitic (with no ferrite) structure of the surface layer and the highest fraction of pearlite in the core. In turn, such a structure evidences the best results of the applied carburizing process.

Along with increasing silicon content, yield stress of the examined specimens also increases and their plasticity declines. This nature of property change confirms the well-known beneficial effect of silicon on solid solution strengthening of ferrite.

The addition of 1% silicon provides an optimum set of properties for the examined sintered steels, with boron obtained by the vacuum carburizing method.

REFERENCES

[1] Binary Alloy Phase Diagrams. 2nd ed. ASM International (OH), 1990
[2] Kunst, H., Schaaber, O.: HTM Härterei-Techn. Mitt., vol. 22, 1967, no. 1, p. 1
[3] Beiss, P., Ruthardt, R., Warlimont, H.: Powder Metallurgy Data. Landolt-Börnstein Online, vol. 2A1. Springer Berlin Heidelberg, 2003
[4] Karwan-Baczewska, J., Rosso, M.: Powder Metall., vol. 44, 2001, p. 221
[5] German, RM., Rabin, BH.: Powder Metall., vol. 28, 1985, p. 7
[6] Madan, DS., German, RM., James, WB.: Prog. Powder Metall., vol. 42, 1986, p. 267
[7] Selecka, M., Dudrova, E. In: Proc. 8th Int. Conf. on Powder Metallurgy. Vol. 3. Piestany, CSFR, 1992, p. 71
[8] Herring, DH., Hansen, PT.: Advanced Materials & Processes, vol. 4, 1998, p. 153
[9] Weber, RG.: Int. J. of Powder Metall., vol. 15, 1983, p. 383
[10] Preisser, F., Seemann, R., Zenker, WR.: Advanced Materials & Processes, vol. 6, 1998, p. 84II
[11] Kula, P., Pietrasik, R., Dybowski, K.: Journal of Materials Processing Technology, vol. 164-165, 2005, p. 876
[12] Minarski, P., Preisser, F., Zenker, WR.: Advanced Materials & Processes, April 2000, p. H23
[13] Tibbetts, GG.: J. Appl. Phys., vol. 51, 1980, no. 9, p. 4813
[14] Eckstein, HJ.: Technologie der Warmebehandlung von Stahl, 1976, Leipzig, 60-67.
[15] Neumann, F., Schenck, H.: Arch. für Eisenhütten, vol. 30, 1959, p. 477
[16] Schenck, H.: Arch. für Eisenhütten, vol. 39, 1968, p. 255
[17] Brown, A., Garnish, ID., Honeycombe, RWK.: Met. Sc. J., vol. 8, 1974, p. 185